This is a repository copy of *A log-normal spectral analysis of inorganic grain-size distributions from a Canadian boreal lake core: Towards refining depositional process proxy data from high latitude lakes*.

White Rose Research Online URL for this paper:
http://eprints.whiterose.ac.uk/99053/

Version: Accepted Version

A log-normal spectral analysis of inorganic grain-size distributions from a Canadian boreal

lake core: Towards refining depositional process proxy data from high latitude lakes.

Gammon P.[1, 2 *], Neville L.A.[2,5], Patterson R.T.[2], Savard, M.M.[3], Swindles G.T.[4]

1   601 Booth St, Natural Resources Canada, Geological Survey of Canada, Ottawa, Ontario,

Canada, K1A 0E8; email: pgammon@nrcan.gc.ca

2   Department of Earth Sciences, Carleton University, Ottawa, Ontario, K1S 5B6

3   Natural Resources Canada, Geological Survey of Canada, Quebec City, Quebec, G1K

9A9

4   School of Geography, University of Leeds, LS2 9JT United Kingdom

5   Now at: Geological Survey of Canada, Calgary, Alberta, T2L 2A7

* Corresponding author

Associate Editor – Daniel Ariztegui

Short Title – Grain size spectral analysis of a boreal lake

ABSTRACT

Better methods for interpreting grain size spectra will enhance current understanding of past transport–depositional processes. A high-resolution inorganic grain-size dataset has been measured from a freeze core extracted from 'Alberta Lake E' a boreal fresh water lake 40 km east of the Athabasca Oil Sands in north-eastern Alberta, Canada. The grain-size spectra are remarkably consistent throughout the core, exhibiting a structure comprising six persistent grain-size distributions below *ca* 250 μm, plus a rare medium-sand distribution. Automated deconvolution of the grain-size spectra produced poor results. Constraining the modes of two of the distributions produced deconvolution solutions that were statistically excellent and consistent with the structure of each spectrum. Statistical analysis of the 'constrained' solutions indicates that deconvolution successfully extracted independent grain-size populations. Conversely, the multimodal spectra generate traditional measures (for example, mean grain size) that are inconsistent combinations of different individual populations, and thus are poor proxies of transport–depositional processes. Alberta Lake E is situated in a boreal wetland landscape where sediment delivery is dominated by overland flow transport during spring melt. This context means that the Alberta Lake E grain-size spectra can be interpreted to reflect: (i) a bedload component transported during short-duration high discharge events that reflect the intensity of the melt; and (ii) a finer suspended load component representing material whose magnitude is controlled by the volume of the spring melt. Stratigraphically, bedload and suspended load populations demonstrate different short-wavelength and long-wavelength cyclicity, suggesting that spring melt is likely to be driven by cyclic external forcing factors. The links between the grain-size spectra and spring melt have potential for generating proxy records that better capture the external controls over spring melt in boreal systems, and the risks associated with these

energetic hydrodynamics. This is exemplified by the coarsest Alberta Lake E distributions, which indicate that more intense spring melt dynamics occurred in pre-historical times.

Keywords: Boreal lake, grain-size analysis, parametric curve fitting, sedimentology, spring melt, stratigraphy

INTRODUCTION

A focus of palaeoenvironmental research is the development of high-resolution palaeoenvironmental reconstructions spanning the last few thousand years (PAGES_2k_Consortium, 2013). High-resolution studies generally require large numbers of analyses of samples that capture, generally via a proxy relationship, an environmental variable of interest. The advent of laser particle analysers (Syvitski, 1991) and microtomes (Macumber et al., 2011) now makes it possible to rapidly generate high-resolution grain-size datasets from fine slices of unconsolidated sediment cores. However, the use of grain-size data as a temporal proxy for environmental processes remains controversial (Dietze et al., 2012; Flemming, 2007; Le Roux & Rojas, 2007; Middleton, 1976; Weltje & Prins, 2007; Xiao et al., 2012). Less controversial, although rarely utilized in palaeoenvironmental time series, is the recognition that most grain-size spectra are composites of multiple overlapping grain-size populations (Bartholdy et al., 2007; Dietze et al., 2013; Le Roux & Rojas, 2007; Qin et al., 2005; Sheridan et al., 1987; Xiao et al., 2012). In such spectra the identification of individual populations is reliant on statistical deconvolution. The most common methods proposed for deconvolving grain-size spectra are: (i) full discrete parametric curve-fitting (e.g. Qin et al., 2005; Sheridan et al., 1987; Xiao et al., 2012); (ii) end-member mixing analysis (EMMA; e.g. Dietze et al., 2012; Dietze et

al., 2013; Ijmker et al., 2012; Weltje & Prins, 2007); and (iii) sediment trend analysis (STA; e.g. Bartholomä & Flemming, 2007; Le Roux & Rojas, 2007; Poizot et al., 2008). Both EMMA and STA have been used mostly to investigate grain-size distributions within a horizontal (single temporal timeframe) two-dimensional context, such as sedimentary facies distributions and their underlying generalized transport–depositional processes. Both of these geostatistical techniques assume that the grain-size distributions of different samples are a reflection of the transport–depositional processes within an area, i.e. the samples are assumed to be in a dynamic relationship and the algorithm employed seeks to uncover that relationship. This assumption is not necessarily valid in temporal studies, where the vertical 1D stratigraphy can capture diverse, unrelated sedimentological processes. Nevertheless, EMMA has been utilized in the analysis of the environmental processes linked to ancient sediments (Dietze et al., 2013; Weltje & Prins, 2003).

In contrast to EMMA and STA, deconvolution via parametric curve fitting is based on the principle that any individual grain-size spectrum represents an amalgam of discrete grain-size populations, each of which was generated by an erosional–depositional–transport mechanism (Ashley, 1978; McCave & Hall, 2006; McLaren & Bowles, 1985; Tanner, 1964; Xiao et al., 2012). Deconvolution procedures aim to identify all of the individual populations within each spectrum. The relative merits of a variety of parametric curve-fitting approaches have been debated at length (for example, tanh, log-normal, log-hyperbolic, Weibull functions, etc.; Bagnold & Barndorff-Nielsen, 1980; Barusseau, 2011; Hajek et al., 2010; Leys et al., 2005; Påsse, 1997; Sun et al., 2002) and it is likely that the best parametric curve fitting approximation is context-specific. Barusseau (2011) summarized the debate well by differentiating between the

end uses of grain size deconvolution: (i) for disciplines such as hydraulic engineering and coastal geomorphology, the grain-size populations need to be deconvolved as accurately as possible because the defined population(s) will be used in subsequent models of sediment dynamics and engineering solutions. Given the complexities of real systems the choice of parametric function for deconvolution needs to be carefully examined (Barusseau, 2011; Flemming, 2007; Molinaroli et al., 2009); (ii) studies that compare grain-size populations (for example, sedimentary facies analysis or time series) are more concerned with variability within and between samples and, consequently, the choice of parametric curve type probably introduces at worst an internal and/or systematic error. The populations derived are therefore inferred to be internally consistent with a qualitative relationship to environmental processes. Nevertheless, some studies have further attributed the deconvolved populations to specific environmental processes (Ashley, 1978; Bartholomä & Flemming, 2007; McCave & Hall, 2006; McLaren & Bowles, 1985; Molinaroli et al., 2009; Tanner, 1964).

Relatively few time-series studies have utilised deconvolved individual grain-size populations (Chen et al., 2013). Instead, time-series studies of grain-size data commonly utilise traditional grain-size summary statistics or specific components (for example, median or mean grain size, percent clay and/or silt and/or sand, end member mixing proportions, etc.) and interpret these as proxy data for the general sediment dynamics (Chen et al., 2013; Dietze et al., 2012; Johnson & McCave, 2008; Wang et al., 2006; Weltje & Prins, 2007). The implicit assumption when using these types of grain-size proxies is that they adequately represent environmental processes.

This study utilizes a novel deconvolution and peak-fitting procedure, which includes constraints on solutions, to extract unimodal log-normal grain-size populations for a subset of the grain-size spectra analysed from a sediment freeze core extracted from 'Alberta Lake E' (ALE); an informally-named lake situated *ca* 40 km north-east of Fort McMurray, Alberta, Canada (Fig. 1). This sample subset is subsequently used as a training set to extend some deconvolved population parameters across the complete ALE grain-size data. The quantitative grain-size proxy data is then combined with a detailed understanding of the sedimentological and physiographic context of ALE to generate a stratigraphic profile of specific bedload and suspended load transport-deposition processes. The deconvolved populations are also compared against traditional proxy data measures such as mean grain size.

METHODS

Sediment collection

A 1.45 m freeze core was collected from Alberta Lake E (ALE) at 3.75 m water depth in September 2010 (latitude 56.87933º; longitude -110.5678º). The coring location was chosen based on water depth, location within the lake, surrounding landscape and substrate type. For further physiographic information on ALE see Supplementary Information. The massive black gyttja sediment remained frozen until sectioning prior to grain-size and other analyses. The core has a ^{210}Pb age model that indicates that the top 30 cm represents the last 150 years (Jautzy et al., 2013).

Grain-size measurements

A purpose-built freeze-core microtome was used to section the ALE core (mostly 2 mm resolution), starting with the 0 to 1 mm surface sample (slice 1) to slice 1451 (n = 701 analyses). Detailed information regarding pre-analysis strategy and treatment methods are documented in the Supplementary Information. Briefly, sediment samples were digested in a heated water bath with 10% v/v% H_2O_2 to remove organics (van Hengstum et al., 2007). Grain-size analysis of digested samples was performed in triplicate with a Beckman Coulter LS 13 320 Laser Diffraction Analyzer (Beckman Coulter Inc., Brea, CA, USA) fitted with a Universal Liquid Medium (ULM) sample chamber. The samples were run in distilled water with an obscuration level of $10 \pm 3\%$, over a measurement range of 0.4 to 2000 μm (Murray, 2002). The laser diffraction data were initially converted to equivalent spherical grain-size volume using the Fraunhofer and Mie diffraction models, and then size-class data were averaged for the triplicate analyses. Gradistat software (Blott & Pye, 2001) was used to extract the mean grain size, medium silt, total silt and fine sand volume percentages from the equivalent spherical grain-size diffraction data.

Grain-size data analysis

Multiple deconvolution methods were trialled (detailed in both the *Results* section below and Supplementary Information). The final deconvolution protocol used was:

1) All grain-size spectra were visually examined to determine the general structure of the spectra (Fig. 2) and to identify any spectra that did not conform to the general spectral structure (Fig. 3). See also SI *Notes 1* and *2*.

2) A subset of 50 samples was chosen for testing different deconvolution and peak fitting combinations. These samples were spaced approximately every 200 mm down core, with at least three contiguous samples chosen from each 200 mm segment. The contiguous samples were specifically chosen to capture the grain-size spectral variability for that 200 mm portion of the core (Fig. 2). This selection method ensured that the sample subset included grain-size spectra that were broadly representative of both the whole core and the most important aspects of grain-size variability, including potential cyclic sedimentation processes.

3) The second-order and fourth-order derivatives of each spectrum within the subset were calculated (Fig. 4) to help identify the positions of populations that are represented by either unambiguous peaks (i.e. peaks with two downward-sloping sides) or changes in slope (inflection points) that are likely to be indicative of the existence of subordinate grain-size populations within the spectrum (cf. Bartholdy et al., 2007; Flemming, 2007; Qin et al., 2005; Xiao et al., 2012). The derivative plots also identify the approximate mode for each of the log-normal distributions, which was noted and used in later steps in the analytical process.

4) The PeakFit® software package (SeaSolve Software Inc.; www.seasolve.com) was used to deconvolute each spectrum in the 50 sample subset. Initial trials used 2, 3, 4 … to 9 log-normal distributions. This trial and error aimed to determine the most suitable number of distributions for each spectrum, an approach also commonly employed in automated log-normal fitting (Xiao et al., 2012) and EMMA (Weltje & Prins, 2007).

5) Optimization of the log-normal distributions within each deconvolution model (termed peak fitting) was also conducted via PeakFit® software. PeakFit uses an iterative 'peak

sharpening' (derivative-based) algorithm whereby a solution is derived and then tested to determine whether any further 'sharpening' produces better or worse least-squares criteria. The iterations were continued until the chi-squared goodness of fit criteria attained values unchanging in the sixth decimal place. Once completed, the fit between the model and measured spectra can be evaluated via the coefficient of determination (r^2), Standard Error (SE), and F-statistic goodness of fit measures (Figs 2 and 3). Overall each deconvolution and subsequent peak optimisation (steps 4 and 5) procedure is similar to methods used by other authors undertaking log-normal deconvolution (Ashley, 1978; Flemming, 2007; Qin et al., 2005; Sheridan et al., 1987; Sun et al., 2002; Xiao et al., 2012).

6) Peak fitting can generate incorrect results by migrating distributions to unrealistic values (Seasolve, 2003) which did occur in these peak fitting models. To correct this problem the mode of distribution 2 was constrained to between 5.0 to 6.5 μm, and that of distribution 5 to >80 μm (the reasons for this are detailed in SI *Note 3*).

7) The reproduction of the basic spectrum structure (i.e. main spectral peaks and troughs align with the main distributions within a solution) was used as a qualitative criterion for acceptance or rejection of different deconvolution models.

8) The deconvolved and peak-fitted model generates the following statistics for each identified log-normal distribution within a spectrum: area, maximum amplitude, modal grain size and the full-width at half the height of the maximum amplitude (FWHH, which is a similar measure to the standard deviation of a distribution).

Extending the deconvolution to the other grain size spectra

To extend the deconvolution analysis across the whole dataset, the 50 deconvolved samples were used as a training set to generate, via least-squares fitting, a polynomial that could estimate, using the size-class data of each grain-size analysis, the area and amplitude statistics for the remainder of the samples (using STATA® statistical software; www.stata.com). Algorithms were generated for the distribution 3 (D3) Area and distribution 6 (D6) Amplitude parameters (SI; Appendix 1). These two examples were then compared to other grain-size measures, such as mean grain size.

RESULTS AND INTERPRETATION

Spectral Deconvolution

Grain-size spectral structure

The grain-size spectra from ALE are exceptionally consistent in their overall structure (Figs 2, SF4 and SF5). From the finest grain size measured (0.4 µm) to *ca* 3 to 4 µm there is a broad low amplitude shoulder or unambiguous peak observed in all spectra (Fig. 2). The area of fine grain sizes between 3 to 4 µm and *ca* 30 µm either contains a single broad peak with a mode between 7 µm and 14 µm Fig. 2A and C), or two clearly distinguished peaks with modes between *ca* 5.0 to 6.5 µm and *ca* 17 to 20 µm (Fig. 2B and D). Generally, samples characterized by overall coarser-grained spectra are those with two clearly distinguished peaks. Between *ca* 30 µm and *ca* 120 µm there is generally a single peak centred around 50 µm. The peak is either approximately symmetrical if it is of high amplitude (Fig. 2D), or it has unequal-sloped sides if of low amplitude (Fig. 2B). In some of the overall finest-grained spectra (i.e. spectra where the 3 to 30 µm area is relatively large), this peak can be reduced to an inflection beside a large finer-

grained peak at 3 to 30 µm (Fig. 2A and C). In these finest grained spectra a small distinct peak occurs at *ca* 90 to 100 µm. However, in most spectra this peak is generally represented by either a broad plateau or shoulder in the *ca* 70 to 120 µm grain size range (Fig. 2B to D). The coarsest grained peak that is common to all of these spectra is centred at *ca* 150 µm. The finer-grained side of this peak is coincident with the *ca* 70 to 120 µm plateau/shoulder and is generally a low-angle slope. The coarser-grained side of the 150 µm peak has an exponential decay slope in virtually all spectra.

Visual examination had previously identified three spectral types (total of eight samples) that diverge from the above structure (Fig. 3). The most common difference (five samples) is the presence of a broad, low-amplitude medium to coarse sand sized population (the '237 mm' sample type; Fig. 3, solid line). The 237 mm sample itself has 7.7% of its total grain-size population in this peak, while the other four samples within this group have <1% of their total population in this peak. Samples with a medium sand peak otherwise exhibit all of the common spectral structural characteristics listed above. The medium sand distribution does not overlap any of the finer-grained distributions. Consequently, it is both easily distinguished and too minor to have been included in the spectral deconvolution and peak fit modelling.

The 691 mm sample has virtually no sand, but otherwise follows the general spectral structure above. This leaves only two spectra ('985 mm' type spectra in Fig. 3) out of the total 701 spectra that substantially diverge from the general spectral structure. These two adjacent samples, at 985 mm and 987 mm, exhibit no fine silt peak, but rather a single coarse silt peak at *ca* 35 µm, a grain size region that is either a spectral low or a shoulder to the *ca* 50 µm silt peak in all other spectra.

Grain-size spectral structure - interpreting the number of distributions

The second-order and fourth-order derivative plots are good indicators of the smallest number of log-normal distributions present (Fig. 4; see also SI *Notes 1* and *2*). For example, in the most fine-grained spectra examined, there is generally an unambiguous peak indicative of a small very fine sand-sized population (mode 80 to 110 μm; Figs 2A and 4A). In coarser-grained spectra this minor population can only be inferred on the basis of an inflection and/or shoulder and/or plateau in this region (compare Fig. 2A to 2D). Second-order and fourth-order derivative plots yield a weak to moderate peak in the very fine sand region (Fig. 4B and C), indicating the presence of a very fine sand-sized population that is essentially hidden by the larger amplitude peaks on either side in coarser-grained samples. The six common distributions observed in the spectral structure are therefore consistent with the six peaks observed within the derivative plots (Table 1).

The trial and error deconvolution and peak fitting procedure used generated fitting statistics that reached their maxima (r^2, F-statistic) or minima (standard error) with a total of six distributions (Fig. 5). Any increase in the number of distributions modelled did one or more of the following: (i) not result in any significant improvement of the fit statistics, and sometimes resulted in a decline; (ii) PeakFit generated near-zero or sometimes negative amplitudes for one or more of the distributions, indicating that the solution does not require those distributions to model the measured data; or (iii) one or more distributions was both wholly within and a minor component of another distribution, indicating that only one single distribution was required in that grain-size region (Figs SF4B and SF4C).

The general spectral structure (Fig. 2), derivative plots (Fig. 4) and deconvolved-peak fitted models (Fig. 5) all indicate that there are seven discrete log-normal grain-size distributions

within these grain-size spectra. The subsequent modelling of this data utilized a six distribution structure to the PeakFit modelling (the six illustrated in Fig. 2, minus the rare '237 mm' type medium sand mode distribution shown in Fig. 3). From smallest to largest these distributions are termed D1 to D6 (see Table 1 for basic statistics). Similarly, the modes of these distributions are labelled M1 to M6, respectively.

Distributions D1 and D6, the finest and coarsest grain populations, respectively, are easily distinguished in virtually all spectra. Of the D2 to D5 distributions the very fine sand distribution (D5) has unambiguous peaks in 45 (6.4%) of the spectra, the other three distributions all have unambiguous peaks in more than 20% of spectra; i.e. all of these distributions are common within the data. The only unambiguous peak excluded from the data is that at 35 μm in the two contiguous anomalous samples at 985 mm and 987 mm down core (0.3% of samples; Fig. 3).

Peak Fitting

Results: Peak fitting generates the best statistical model without considering other constraints, such as spectral structure or derivative plots, and in an automated mode has a known tendency to migrate distributions (Seasolve, 2003). Peak fitting of the ALE grain-size data without any constraints on the distributions encountered this problem (see SI *Note 3* for unconstrained peak fitting results). To resolve this problem, without unduly limiting the potential peak fitting solutions, required two constraints: (i) to force PeakFit to distinguish between the coarse silt and very fine sand distributions the M5 (very fine sand mode) was constrained to >80 μm, consistent with the minimum M5 of 83.2 μm observed in the derivative plots (Fig. 4); and (ii) to force solutions to better approximate the bimodal structure of the 3 to 30 μm range, M2 was

constrained to 5.0 to 6.5 µm. This range matched that observed in the derivative plots (Fig. 4). The alternative of constraining the range of the M3 was trialled but found to be less successful, as gauged by generally poorer fitting statistics found with finer-grained samples. This was probably due to the best M3 estimate of 17 to 20 µm being derived from coarser-grained samples, which was probably an inappropriate M3 constraint for finer-grained spectra (Fig. 2; Table 1). Both the D2/D3 and D5 migration related issues are essentially a product of trying to find the best statistical model for strongly overlapping distributions, which is not a problem restricted to PeakFit or grain-size data, and usually requires additional information to be fully successful (Bah et al., 2009; Flemming, 2007). A statistical comparison between the unconstrained and constrained results is given in SI *Note 4*.

Area and peak amplitude are measures of the overall size of the distribution (Hartmann, 2007), and the basic statistics for the constrained peak fits indicate that D2, D3 and D4 are the most important grain-size populations in these spectra (Table 1). In contrast the mode and FWHH are measures that reflect the position and shape, respectively, of each distribution within a spectrum (Hartmann, 2007). Hence the combined basic statistics of the deconvolution peak fit models (Table 1) are a representation of the position, shape and size of each distribution. These characteristics combined reflect the general spectral structure; i.e. strongly overlapping D2 and D3; weakly overlapping D3 and D4; strongly overlapping D4 and D5; D1 and D6 weakly overlapping D2 and D5, respectively (Figs 2, 3 and SF4). Both the FWHH and Aspect Ratio (mode-normalised FWHH) are measures of the distribution width and both demonstrate the generally poor sorting for D1 to D3, moderate sorting for D5 and D6 and moderate to moderately well-sorted D4 (Table 2; Friedman, 1962).

Spearman rank correlation analysis of the area, amplitude, mode and FWHH measures

for the constrained model solutions provide an indication of how these parameters co-vary across the sample suite (Table 2). There are two striking features of the correlations between the size parameters of the distribution (Table 2A and 2B): (A) area and amplitude for D1 to D3 are negatively correlated with those of D4 to D6; and (B) area and amplitude for D4 to D6 are all strongly positively correlated with one another. D1 to D3 exhibit no consistent cross-correlations with the only substantial correlation being a strong negative one between D2 and D3 areas. The position (mode) and width (FWHH) of most distributions are generally uncorrelated (Table 2C and 2D). A notable exception to this is the positive correlation between mode and FWHH for D3 and D4.

Interpretation: Understanding the impact of constrained peak fitting is clearly important to the overall interpretation of these spectra. Constrained–unconstrained correlations indicate that the solutions for D4 and D6 are relatively robust irrespective of constraints, whilst all other solutions are variably impacted, D2 being the most impacted (see SI Note 3 for detailed discussion).

Log-normal distributions have long been recognized as an approximation of the individual grain-size populations, in that each log-normal distribution essentially reflects the transport-deposition processes that controlled that population (Ashley, 1978; Flemming, 2007; Le Roux & Rojas, 2007; Middleton, 1976; Middleton, 1990; Xiao et al., 2012). The strong positive and negative correlations between area and amplitude indicate fundamental scale-based relationships between the different populations within these spectra (Table 2). Scale parameters reflect the magnitudes of the different transport–depositional processes represented by the individual distributions (Hartmann, 2007), suggesting there are important magnitude relationships revealed by this deconvolution methodology.

In contrast to the scale parameters, the position (mode) and shape (FWHH) parameters are a reflection of the hydraulic processes that govern the grain-size populations (Hartmann, 2007; Kranck et al., 1996a; Kranck et al., 1996b; Middleton, 1976; Påsse, 1997; Sheridan et al., 1987). The general non-correlation, with a notable exception of the D3 to D4 mode-FWHH relationships, of the position and shape parameters of these distributions indicates that for the most part these populations are not generally linked at the hydrodynamic process level (Table 2). This suggests that the deconvolution and peak fitting procedure used herein did successfully separate discrete grain-size populations that were each controlled by a distinctive set of erosion–transport–depositional processes (this is further examined in the *Discussion*). Overall the area, amplitude, mode and FWHH parameters of grain-size distributions are important evidence for understanding the relationships between the different parameters, but are generally little used in stratigraphic studies utilising grain-size data.

Extending the deconvolution to non-deconvolved grain size spectra

The deconvolved and peak-fitted spectra represent a subset of the grain-size spectra measured in the study that are assumed to capture the spectral variability The original grain-size frequency-class measurements were used as a training set against which the D6 amplitude and D3 area parameters were regressed as dependent variables to yield polynomial equations that approximate the deconvolution statistic (Fig. 6; SI Appendix 1). The polynomial equations were used to extend the D6 Amplitude and D3 Area parameters across all samples except the two anomalous 'type 985 mm' spectra. The Spearman rank correlation coefficients between the original deconvolution statistics and their polynomial approximations were 0.97 and 0.98 for D3 Area and D6 Amplitude, respectively.

DISCUSSION

Spectral deconvolution and peak fitting

The deconvolution of ALE grain-size spectra into seven distributions was relatively straightforward due to the consistent stratigraphic spectral structure for all but two adjacent samples (Fig. 4). Conversely, peak fitting D1 to D6 of the spectra was not straightforward due to the degree of overlap between D1 to D3 and D4 to D5 distributions (Figs 2 and SF4). As noted by many authors, there is no single solution when deconvolving and peak fitting strongly overlapping distributions within a spectrum, as also demonstrated by the excellent fit-statistics for both constrained and unconstrained solutions (Ashley, 1978; Bagnold & Barndorff-Nielsen, 1980; Bah et al., 2009; Flemming, 2007; Middleton, 1990; Påsse, 1997; Sun et al., 2002; Weltje & Prins, 2007). Most grain-size deconvolution studies lack independent data for determining which peak fitting solution is best, as is the case for ALE. Consequently, choosing a preferred peak fit is a subjective judgment based upon a prioritization of the accuracy and importance of the different pieces of quantitative information within one or more spectra. The preferred solution is that which most accurately recreates the highest priority piece of quantitative information (Leys et al., 2005). For the overlapping D1 to D3 and D4 to D5 grain-size ranges in the ALE spectra, the preferred solution was the one that reproduced the D2 and D5 modes exhibited in spectra hosting unambiguous D2 and D5 peaks. There is considerable sedimentological support for using the mode as the determining factor for anchoring grain-size population positions (Bah et al., 2009; Barusseau, 2011; Kranck et al., 1996b; Påsse, 1997; Sheridan et al., 1987; and the many references therein). There is also mathematical support for prioritizing the distributional mode as the most accurate quantitative information when deconvoluting grain-size data (Hajek et al., 2010; Leys et al., 2005; Lwin, 2003; Weltje & Prins,

2007). Both of these lines of support highlight the mode as the single positioning parameter within both log-normal and other parametric curve-fitting approaches. In relation to peak fitting and the potential migration of modes to unrealistic values, the best summary encountered is: "It is therefore especially important that centre values be constrained and not be permitted unlimited freedom of movement." (the term 'centre' indicates mode; Seasolve, 2003). Many grain-size deconvolution and peak fitting studies do not constrain the modal position, although the capacity to constrain modes in EMMA is a notable exception (Dietze et al., 2012; Weltje & Prins, 2007).

Conceptual sedimentological context for Alberta Lake E (ALE)

An understanding of the sedimentological context of ALE is required to assess the significance of both the observed grain-size populations and their stratigraphic variation. The first-order factors controlling ALE sedimentology include: (A) the hydrological regime controlling the run-off volume and intensity; (B) the climatic regime, which for this area is primarily the distribution of water through the seasonal cycle; (C) the landscape surrounding ALE, which controls the erosion-transport parameters; (D) the current action within the lake, which controls the internal distribution and/or redistribution of the grains entering the lake; (E) bioturbative mixing – being massive black gyttja, the ALE core would ordinarily be assumed to be pervasively bioturbated. However, there is a lack of fine-grained sand in the '691 mm' type sample, even though there are normal amounts of fine sand in the spectra of samples at 689 mm and 693 mm. Similarly, 2 mm spaced samples either side of the five '237 mm' type samples contain no medium sand. This suggests a bioturbation mixing depth <2 mm; and (F) the grain-size distribution and mineralogy of the source regions, which controls what grain sizes are available for erosion–transport–deposition. Specific grain-size data for the source regions within

the Fort McMurray area are limited to coarse size-class data, which indicates that all class sizes are available (Appendix 4 of Andriashek, 2003; see also McLaws, 1980). The surficial geology of the area is primarily comprised of tills, which in general contain a wide variety of grain sizes. It is therefore considered unlikely that there is a deficiency in any particular grain size class within the source region, and criterion '(vi)' is not considered to have been a controlling factor in the ALE grain size spectra.

The hydrological record indicates the ALE region hosts a typical hydrological cycle for a boreal region (see *Physiography* section in SI). The ALE coring site is also fully surrounded by wetlands (see SI), and run-off of all types will have first traversed the wetlands before entering ALE. In boreal wetland environments the seasonal hydrological pattern is markedly partitioned (Fang et al., 2010; Pomeroy et al., 2007; Shook et al., 2013). Spring melting generates overland flow due to frozen subsurface organic soils that prevent or severely inhibit infiltration of the large volumes of snow melt water that is delivered over relatively short time spans (Carson et al., 1973; Gibson et al., 1993; Gray et al., 2001; Metcalfe & Buttle, 1999; Shook et al., 2013). Sedimentological measurements of spring run-off indicate that the discharge volume generally controls the volume of sediment delivery (Cockburn & Lamoureux, 2008a; Cockburn & Lamoureux, 2008b; Laudon et al., 2007; Metcalfe & Buttle, 1999; Metcalfe & Buttle, 2001), whilst the run-off 'intensity' (i.e. velocity and run-off rate) controls the delivered grain size (McDonald & Lamoureux, 2009; McDonald et al., 2010). Combined, these studies demonstrate that the spring melt is a heterogeneous period that is mostly comprised of short peak-flow time periods, interspersed within and succeeded by recessional streamflow of significantly lower discharge volume and velocity. Commonly the peak flow events during spring melt are short-duration high discharge events driven by a rain and/or high temperature event (see figure 5 of

McDonald & Lamoureux, 2009).

In contrast, the summer–autumn–winter period is dominated by plant evapotranspiration and/or ongoing subsurface flow. During summer, boreal slope soils are mostly dry and take considerable wetting before they export water (Gibson et al., 1993; Redding & Devito, 2008), whilst the wetlands act as a sink for precipitation (Kværner & Kløve, 2008; Lyon et al., 2012; McNamara et al., 2005; Redding & Devito, 2008). Nevertheless, summer thunderstorms are a component of northern boreal summers and represent a potential mechanism for overwhelming the holding capacity of the wetland and thereby initiating surface run-off (Kværner & Kløve, 2008). Redding & Devito (2008) estimated that for northern Albertan hill slopes, such as those of the Firebag Hills Uplands near ALE, the return period for summer storms capable of generating >1 mm of surface run-off (i.e. very minor flow) from the soil was *ca* 25 years. Wetlands would probably further attenuate the volumes and velocities of storm-generated summer–autumn run-off, thereby extending this return periodicity significantly (i.e. even anomalously large summer storm streamflow events would be strongly attenuated and not produce significant run-off into a wetland-surrounded lake such as ALE). Overall it is highly likely that summer surface run-off to ALE is negligible for the majority of years. However, if summer run-off were to occur, the wetlands surrounding ALE would probably preferentially capture bedload and thus skew the sediment delivery to suspended load material. A grain-size spectrum similar to that of the '691 mm type' sample in Figure 3 may reflect such a situation.

Easterly winds greater than 15 m/s over the 1 km fetch between the eastern shore of ALE and the coring site could conceivably generate high frequency wind waves *ca* 10 cm high (Hamilton & Mitchell, 1996; Young & Verhagen, 1996). However, the wind record for the

region indicates that easterly winds of speeds above 8 m/s are rare for the area. Case studies of lake high-frequency wind waves indicate a lack of reworking in benthic sediments at 3.5 m water depth (Hofmann et al., 2008; Jin & Ji, 2004; Luettich et al., 1990). Combined flow in lakes is generally generated via the coupling of inflow, outflow and wind. Much of the non-wave current activity is secondary effects of the waves and inflow regimes themselves (for example, reflected waves and coriolis circulation, Jin & Ji, 2004; Soulsby et al., 1993). The limited fetch and seasonally-restricted run-off period of ALE make it unlikely that combined flow is significant outside of the spring melt run-off period. The floating riparian fen that rims the ALE shoreline attests to the lack of significant wave and current activity in the lake. Factor 'D' is therefore considered insignificant for a small lake, such as ALE, which is consistent with findings elsewhere.

The physiography surrounding ALE indicates that inorganic sediment will be derived from the northern hills and southern margins, plus potentially from the west, and delivered via the inlet channel (see SI, Fig. SF1). The stream channels entering ALE are all either well north-east (downstream and across the lakebed subaquatic channel) of the coring site, or discontinuous wetland channels. The single inlet channel to ALE, which is near the coring site, and thus potentially an important sediment delivery system, is both discontinuous and embedded within extensive aquatic vegetation (reeds). It is probably a sink rather than a conduit, certainly for bedload particles. Overall, the lack of effective streams near the coring site means that focused point-source sediment delivery via stream channels is likely an insignificant method of bedload sediment delivery to the ALE coring site. Spring-melt overland flow, which has been demonstrated to be the predominant method of surface water flow across frozen wetlands (Gibson et al., 1993; Metcalfe & Buttle, 1999; Shook et al., 2013), is considered the most

important sediment delivery mechanism to ALE.

As they apply to ALE, hydrology (factor A above), seasonal climate (factor B) and landscape characteristics (factor C) can be mostly considered to predominantly reflect the sediment delivery associated with the spring melt as has been found for other boreal lakes (Carson et al., 1973; Fang et al., 2010; Gray et al., 2001; Laudon et al., 2007; Lyon et al., 2012; McNamara et al., 2005; Metcalfe & Buttle, 1999; Redding & Devito, 2011; Redding & Devito, 2008). Thus, the grain-size parameters identified within these spectra can be considered to be indicators or proxies for spring melt sediment dynamics.

Alberta Lake E grain-size populations – interpretation of processes

The ALE grain-size spectral structure is consistent throughout the entire core (Figs 2 and SF5), suggesting that the seven log-normal distributions (six consistent, one rare) represent a suite of independent grain-size populations and processes that were persistent throughout the time period represented by the core. However, associating individual grain-size populations with specific processes is difficult and prone to error without corroborating process-based data. Nonetheless, the conceptual sedimentological framework above provides some limits as to what the grain-size analysis herein may represent (see also SI *Note 5*). Distribution D1 is consistent with clay-sized suspended load material. The unique sedimentological properties of clay enable some confidence in its definition (Johnson & McCave, 2008; McCave et al., 1995a; Xiao et al., 2012). Distribution D2 is probably inorganic long-term suspended load material (Chang et al., 2007; Chang et al., 2006; Law et al., 2008; Slattery and Burt, 1997).The D1 and D2 distributions are both likely to be influenced by dissociation of aggregated flocs or particles during laboratory analysis, although the pre-treatment methods used here were designed to minimize this effect

(see SI; McConnachie & Petticrew, 2006). The strong positive correlation between D1 and D2 amplitudes (but not areas) indicates there is some correspondence between the magnitudes of these two populations (Table 2). However, the non-significant mode correlation and strong negative correlation for D1 and D2 FWHHsuggest that these populations do represent different suspension processes (for example, low density clay flocs versus mineral grains kept in suspension via turbulence).

Distribution D3 covers the size range for 'sortable silts' which have received considerable research attention (see Hamm & Dade, 2013). These are thought to be silt-sized grains that travel close to the bed under relatively low shear stress (Chang et al., 2007; Hamm & Dade, 2013; Johnson & McCave, 2008; Law et al., 2008; McCave et al., 1995b; Molinaroli et al., 2009). Turbulence in the bed boundary layer keeps these particles in suspension and they undergo progressive sorting as flow decelerates (McCave et al., 1995b; Middleton, 1976). The moderate mode and FWHH correlations between D2 and D3 indicate that a portion of the D2 grains were potentially travelling as sortable silt-sized aggregates that were disaggregated post-deposition, as has been observed elsewhere (Table 2; SI; Chang et al., 2006).

Distribution D4 is moderately to moderately well-sorted, suggesting that these grains were probably influenced by progressive sorting and are therefore likely to be bedload transported particles. It is the most consistent of all the populations with a relatively narrow range of modes, aspect ratios and FWHH statistics (Table 1). The strong spectral minimum between D3 and D4 probably demarcates the boundary between suspension and bedload sedimentology. Process-based studies indicate that the finest-grained bedload population is generally related to saltation processes (Ashley, 1978; Barusseau, 2011; Chang et al., 2006; Hamm & Dade, 2013; Law et al., 2008; Middleton, 1976; Sheridan et al., 1987; Singer &

Anderson, 1984). Distributions D3 and D4 have significant positive correlations between their position and shape parameters (mode and FWHH; Table 2C and 2D), suggesting that the sedimentological processes controlling these two populations are related. This is consistent with both being related to benthic boundary layer turbulence, which strongly controls the transport and progressive sorting of both sortable silt and saltating particles (Hamm & Dade, 2013; Singer and Anderson, 1984).

Singer & Anderson (1984) documented four populations within bedload transport that in order of increasing grain size were: (i) 'intermittent suspension' (equivalent to what nowadays would be considered suspended load sortable silt rather than bedload); (ii) saltation; (iii) finer-grained traction population; and (iv) coarser-grained traction population. These authors demonstrated that the relative magnitude of these bedload populations varies dependent upon the transport conditions, but for bedload sediment undergoing progressive sorting in a decelerating flow the relationship is saltation > coarser-grained traction population > finer-grained traction population. The relative abundance of the bedload populations at ALE is similar with D4 > D6 > D5. It is consistent with bedload delivery to the ALE coring site probably being decelerating nepheloid layers (discussed further below; Best et al., 2005; Chambers & Eadie, 1981; Cockburn & Lamoureux, 2008b; Singer & Anderson, 1984). In this context D5 and D6 are both likely to be traction processes (for example, perhaps rolling versus sliding).

Alberta Lake E grain-size record

The sedimentological context of ALE indicates that the ALE situation is a relatively simple particle delivery system dominated by the hydrological dynamics of spring melt. This simplicity is probably a primary reason why the spectral structure is so remarkably uniform throughout the core.

Bedload delivery of inorganic sediment (D4 to D6, plus medium sand D7) predominantly occurs during the higher-energy events within the spring melt, which generally occur during the earlier portions of the nival period (McDonald & Lamoureux, 2009; McDonald et al., 2010). Therefore the D4, D5 and D6 spectral measures (mode, amplitude, area and FWHH) can conceptually be considered as proxy measures of different aspects of the spring thaw intensity. For example, the magnitude parameters area and amplitude of log-normal grain-size populations are generally interpreted as a proxy for the sum energy of the process (or processes) that gave rise to that grain-size distribution (Ashley, 1978; Kranck et al., 1996a; Middleton, 1976; Molinaroli et al., 2009; Syvitski, 1991; Tanner, 1983). The year 1990 hosted a high nival peak streamflow (Fig. SF2B), which by this conceptual framework should equate to a relatively high D6 Amplitude in contrast to 1991, which should conceptually equate to a relatively low D6 Amplitude. The ^{210}Pb age model for ALE (Jautzy et al., 2013) does indeed suggest that this is the case (Fig. 6A). The age model also indicates that the regional floods of 1979 and 2007 seem to be represented by anomalously high D6 Amplitude values (maximum streamflows at the Clearwater above Christina station of 366 m^3/s and 299 m^3/s, respectively). However, the highest values for D6 Amplitude occur deep in the core, suggesting that for the oil sands area there is the potential for higher intensity spring melt conditions than captured by current instrumental records.

The finer-grained suspended load populations (D1 to D3) are probably deposited throughout the overland-flow period (Cockburn & Lamoureux, 2008a; Cockburn & Lamoureux, 2008b; Laudon et al., 2007; Metcalfe & Buttle, 1999; Metcalfe & Buttle, 2001). Overland flow occurs in both the nival run-up and through the earliest portions of the recession, eventually ceasing as the wetlands change from being a zone of bypass to a zone of attenuation for overland

flow. Conceptually there should be a relationship between run-off volumes and D1 to D3

population parameters. However, there is no difference between the D3 Area values for 1990

versus 1991, and these values are only slightly lower than that of the 1979 flood year (Fig. 6E).

Given the conceptual framework and the recessional curves (Fig. SF2B), the similarity of the D3

Area between these three years could qualitatively be assessed as due to similar volumes of run-

off occurring in each of those years. The changing wetland dynamic, from sediment bypass to

sink, is a function of wetland thaw rate and can be highly variable from year to year (Fang et al.,

2010). This change is not captured by any instrumental record, hence an accurate calibration of

the D1 to D3 parameters against instrumental run-off volumes is not currently possible. It would

require quantitative data on the mechanics and timing of the wetland bypass to sink transition.

Nonetheless, the correlations between the D1 to D3 population measures do suggest that these

are proxy measures of spring thaw discharge volume, and their stratigraphic series thus provide a

succession of relative spring thaw discharge volume variation.

The consistency of the spectral structure, plus the observed correlations between the

distributions, indicates that the stratigraphic succession of D1 to D6 parameters reflects relative

changes in the spring melt depositional processes in ALE. As examples, Figure 6 plots D6

Amplitude and D3 Area measures, as approximated using the polynomial equations, through the

whole core (Appendix 1). These two parameters vary differently throughout the core (as also

indicated by their non-correlation; Table 3). For example, the nine-point average value of D6

Amplitude decreases substantially down core from 0 mm to *ca* 600 mm, whilst there is

essentially no change in D3 Area over the same interval. Conversely, there are substantial

increases and decreases in the moving average of D3 Area (a relative proxy for spring melt

volume) in the bottom half of the core, an interval where D6 Amplitude (which represents nival

peak flow) is relatively stable. This suggests that these two proxies include long-wavelength oscillations.

Superimposed on the longer wavelength oscillations are distinct shorter-wavelength oscillations (for example, *ca* 300 to 600 mm down core; Figs 6 and SF5), which, indicates that spring melt processes are considerably more variable in times past than for the more recent upper *ca* 200 cm (Fig. SF5). This can also be seen in Figure 2B to D, which demonstrates three adjacent grain-size spectra that represent a single high amplitude and frequency cycle at *ca* 500 mm down core (see also Fig. SF5). The variability in both short-wavelength and long-wavelength cyclicity of these spring melt proxy measures probably reflect an overarching climatic control on the spring melt dynamics, as has been found in other studies (e.g. Anderson, 2012; Campbell, 1998; Cockburn & Lamoureux, 2007; Dietze et al., 2013; Fisher, 2011; Holz et al., 2007). If so, this would imply that the climate mechanisms that control the spring melt are important for understanding the hydrological cycle of the area, including the environmental risks that the high-frequency oscillations and long-term average changes of these proxy data pose to the region.

Grain-size populations versus traditional grain-size measures at Alberta Lake E

In depth or time series analysis of grain size proxy data it is implicitly assumed that the grain-size measure used is related to the depositional environment in a systematic relationship. For example, a common measure used is mean grain size, which is inferred to be the average of the depositional processes for the time period encompassed by the sample (two of many examples are Chen et al., 2013; Sonnenburg et al., 2013). Stratigraphic variation of the proxy data is further inferred to be a measure of the variation of the depositional processes over time.

The process variables generated through the deconvolution and peak fitting, and their subsequent approximations across the whole dataset, can be compared against more traditional grain-size proxy measures such as mean grain size, total silt, etc. The grain-size range of the D6 population closely corresponds to that of the fine sand population, and there is minimal overlap of the D6 population with D5 and D4 populations. This somewhat unlikely coincidence means that the fine sand component of the original grain-size data should correlate well with D6 amplitude, which it does (Table 3; Figs 6A, 6B and 7A).

The grain-size range of D3 approximates that of fine plus medium silt (8 to 32 µm), plus a small contribution from very fine silt. There are no traditional grain-size measures that approximate this range, the closest being fine or medium silt measures. A more nuanced but still traditional approach could be to sum the size-class data for 8 to 32 µm, although the fine silt region of strong overlap between D2 and D3 means the size-class data in this region is inherently a multi-distributional composite. Taking medium and total silt as standard traditional summary measures is clearly insufficient as both of these correlate relatively poorly with D3 Area at the individual sample level, and only modestly using a nine point smoothing average (Table 3, Figs 6D, 6E, 6F and 7C). Comparing D3 against fine plus medium silt does considerably worse than just medium silt, primarily because of the strong overlap with D2 in the fine silt range. Interestingly, total silt correlates better, but in a negative sense, with D6 Amplitude. This is probably an effect of the statistical closure of the raw class-size data (*sensu* Atkinson, 1986), whereby the sand component (mainly D6 because D5 is small) plus the total silt component (D2 to D4) sum to near 100% (the D1 clay population being, like D5, a relatively small component of the system).

There is a relatively high correlation between mean grain size and D6 Amplitude, and a weak, but statistically significant, correlation between mean grain size and D3 Area (Table 3, Figs 6A, 6C, 6E and 7B). The D6 population, despite having lower amplitude than D3, occurs across a much broader range of grain sizes (a range of *ca* 125 μm for D6 compared to *ca* 30 μm for D3). Therefore, D6 is generally the larger of the two populations with a commensurately higher impact on the mean grain size. Nonetheless, the correlation to D3 mean grain size is influenced by both bedload and suspended load components. The bedload:suspended load ratio changes on a sample to sample basis, and consequently mean grain size has no consistent relationship to the depositional processes that operated at ALE.

With careful selection, traditional grain-size class distinctions can provide proxy data that reflects depositional processes (for example, at ALE the fine sand measure is a good approximation for the D6 bedload population; Fig. 7A; Table 3). However, if the goal of using a grain-size measure is to generate a proxy measure for depositional processes, then traditional summary measures are commonly a composite of different portions of one or more depositional processes. In stratigraphic or time-series studies, such a composite grain-size measure will yield proxy data points that contain variable and non-uniform proportions of different transport–depositional processes. Essentially this is introducing error into the proxy measure. Whether this error is sufficient to mask the overarching controls within the system, such as climatic forcing, will probably be context-specific.

CONCLUSIONS

A high-resolution grain-size dataset has been obtained from a 1.45 m freeze core collected from a boreal lake (termed Alberta Lake E 'ALE') in north-eastern Alberta, Canada. A novel approach to deconvolving this data into individual log-normal grain-size populations demonstrates:

1) Automated deconvolution and peak fitting failed to yield sedimentologically realistic results. Combining second and fourth derivative-derived modal constraints with an iterative deconvolution and peak fitting procedure yielded realistic solutions that were consistent with the structure of the grain-size spectra.

2) Statistical analysis of the magnitude (area and amplitude), position (mode) and shape (FWHH) parameters of the deconvolved log-normal distributions can assist in determining the validity of the procedure and relationships between the different distributions. In this study positive correlations between the magnitude parameters in the data suggest overarching environmental controls on the processes; whilst non-correlations between the position (mode) and shape (FWHH) parameters suggest that independent transport–depositional processes are reflected by the extracted log-normal distributions.

3) Overall, given that there are an infinite number of solutions when deconvolving grain-size spectra, and that most stratigraphic grain-size series lack independent data to verify the best solution, this method delivers a more objective and explicit method for prioritizing which spectral parameters deliver the most consistent, statistically defensible and sedimentologically realistic solutions. In this study the priority information was the modes of the different distributions and the basic spectral structure exhibited throughout the dataset.

Alberta Lake E is situated in a sub-humid, boreal, flat, wetland environment. Sediment delivery to ALE occurs via surface overland flow run-off during spring melt, a function of a flat, frozen, impermeable subsurface that essentially bypasses the high melt volumes. In contrast, the wetlands act as a precipitation and sediment particle sink during the summer growing season. This means:

4) The consistent grain-size spectral structure throughout the core is probably a reflection of this relatively simple sedimentological context; whereby inorganic grains are only delivered by overland flow during spring snow melt.

5) Conceptually the grain-size spectra can be interpreted as measures of both the intensity of spring melt (bedload component) and the volume of spring melt (suspended load component).Thus the discrete and consistent deconvolved grain-size populations can be qualitatively linked to specific environmental processes throughout the stratigraphic series.

6) Comparison of the deconvolved grain-size populations against traditional measures of grain size (for example, mean grain size, total silt) demonstrate that the traditional measures are generally composites of different grain-size populations that therefore contain a component of random error. Deconvolved populations probably yield better proxy data for time-series and stratigraphic analysis.

7) Stratigraphic series using two parameters from the deconvolved populations demonstrate that ALE has undergone both long-wavelength and short-wavelength oscillations for both spring melt intensity and spring melt volume. Further research could perhaps calibrate and quantify how well these populations capture these spring melt dynamics.

ACKNOWLEDGEMENTS

REFERENCES

Anderson, L. (2012) Rocky Mountain hydroclimate: Holocene variability and the role of insolation, ENSO, and the North American Monsoon. *Global and Planetary Change*, **92-93,** 198-208.

Andriashek, L.D. 2003. Quaternary geological setting of the Athabasca Oil Sands (in situ) area, north east Alberta, Energy Resources Conservation Board, Alberta Geological Survey : Edmonton, AB, Canada, Canada.

Ashley, G.M. (1978) Interpretation of polymodal sediments. *Journal of Geology*, **86,** 411-421.

Atkinson, A.C. (1986) Masking unmasked. *Biometrika*, **73,** 533-541.

Bagnold, R.A. and Barndorff-Nielsen, O. (1980) The pattern of natural size distributions. *Sedimentology*, **27,** 199-207.

Bah, A.R., Kravchuk, O. and Kirchhof, G. (2009) Fitting performance of particle-size distribution models on data derived by conventional and laser diffraction techniques. *Soil Science Society of America Journal*, **73,** 1101-1107.

Bartholdy, J., Christiansen, C. and Pedersen, J.r.B.T. (2007) Comparing spatial grain-size trends inferred from textural parameters using percentile statistical parameters and those based on the log-hyperbolic method. *Sedimentary Geology*, **202,** 436-452.

Bartholomä, A. and Flemming, B.W. (2007) Progressive grain-size sorting along an intertidal energy gradient. *Sedimentary Geology*, **202,** 464-472.

Barusseau, J.P. (2011) Influence of Mixtures of Grain-Size Populations on the Parametric and Modal Characteristics of Coastal Sands (Hérault, Mediterranean Sea, France). *Journal of Sedimentary Research*, **81,** 611-629.

Best, J.L., Kostaschuk, R.A., Peakall, J., Villard, P.V. and Franklin, M. (2005) Whole flow field dynamics and velocity pulsing within natural sediment-laden underflows. *Geology [Boulder]*, **33,** 765-768.

Blott, S.J. and Pye, K. (2001) GRADISTAT; a grain size distribution and statistics package for the analysis of unconsolidated sediments. *Earth Surface Processes and Landforms*, **26,** 1237-1248.

Campbell, C. (1998) Late Holocene Lake Sedimentology and Climate Change in Southern Alberta, Canada. *Quaternary Research*, **49,** 96-101.

Carson, M.A., Taylor, C.H. and Grey, B.J. (1973) Sediment production in a small Appalachian watershed during spring runoff: the Eaton Basin, 1970-1972. *Canadian Journal of Earth Sciences*, **10,** 1707-1734.

Chambers, R.L. and Eadie, B.J. (1981) Nepheloid and suspended particulate matter in south-eastern Lake Michigan*. *Sedimentology*, **28,** 439-447.

Chang, T.S., Flemming, B.W. and Bartholomä, A. (2007) Distinction between sortable silts and aggregated particles in muddy intertidal sediments of the East Frisian Wadden Sea, southern North Sea. *Sedimentary Geology*, **202,** 453-463.

Chang, T.S., Joerdel, O., Flemming, B.W. and Bartholomä, A. (2006) The role of particle aggregation/disaggregation in muddy sediment dynamics and seasonal sediment turnover in a back-barrier tidal basin, East Frisian Wadden Sea, southern North Sea. *Marine Geology*, **235,** 49-61.

Chen, Y., Chen, S., Liu, J., Yao, M., Sun, W. and Zhang, Q. (2013) Environmental evolution and hydrodynamic process of Dongping Lake in Shandong Province, China, over the past 150 years. *Environmental Earth Sciences*, **68,** 69-75.

Cockburn, J.M.H. and Lamoureux, S.F. (2007) Century-scale variability in late-summer rainfall events recorded over seven centuries in subannually laminated lacustrine sediments, White Pass, British Columbia. *Quaternary Research*, **67,** 193-203.

Cockburn, J.M.H. and Lamoureux, S.F. (2008a) Hydroclimate controls over seasonal sediment yield in two adjacent High Arctic watersheds. *Hydrological Processes*, **22,** 2013-2027.

Cockburn, J.M.H. and Lamoureux, S.F. (2008b) Inflow and lake controls on short-term mass accumulation and sedimentary particle size in a High Arctic lake: implications for interpreting varved lacustrine sedimentary records. *Journal of Paleolimnology*, **40,** 923-942.

Dietze, E., Hartmann, K., Diekmann, B., Ijmker, J., Lehmkuhl, F., Opitz, S., Stauch, G., Wünnemann, B. and Borchers, A. (2012) An end-member algorithm for deciphering modern detrital processes from lake sediments of Lake Donggi Cona, NE Tibetan Plateau, China. *Sedimentary Geology*, **243-244,** 169-180.

Dietze, E., Wünnemann, B., Hartmann, K., Diekmann, B., Jin, H., Stauch, G., Yang, S. and Lehmkuhl, F. (2013) Early to mid-Holocene lake high-stand sediments at Lake Donggi Cona, northeastern Tibetan Plateau, China. *Quaternary Research*, **79,** 325-336.

Fang, X., Pomeroy, J.W., Westbrook, C.J., Guo, X., Minke, A.G. and Brown, T. (2010) Prediction of snowmelt derived streamflow in a wetland dominated prairie basin. *Hydrol. Earth Syst. Sci.*, **14,** 991-1006.

Fisher, D.A. (2011) Connecting the Atlantic-sector and the north Pacific (Mt Logan) ice core stable isotope records during the Holocene: The role of El Niño. *The Holocene*, **21,** 1117-1124.

Flemming, B.W. (2007) The influence of grain-size analysis methods and sediment mixing on curve shapes and textural parameters: Implications for sediment trend analysis. *Sedimentary Geology*, **202,** 425-435.

Friedman, G.M. (1962) On Sorting, Sorting Coefficients, and the Lognormality of the Grain-Size Distribution of Sandstones. *The Journal of Geology*, **70,** 737-753.

Gibson, J.J., Edwards, T.W.D. and Prowse, T.D. (1993) Runoff generation in a high boreal wetland in northern Canada. *Nordic Hydrology*, **24,** 213-213.

Gray, D.M., Toth, B., Zhao, L., Pomeroy, J.W. and Granger, R.J. (2001) Estimating areal snowmelt infiltration into frozen soils. *Hydrological Processes*, **15,** 3095-3111.

Hajek, E.A., Huzurbazar, S.V., Mohrig, D., Lynds, R.M. and Heller, P.L. (2010) Statistical Characterization of Grain-Size Distributions in Sandy Fluvial Systems. *Journal of Sedimentary Research*, **80,** 184-192.

Hamilton, D. and Mitchell, S. (1996) An empirical model for sediment resuspension in shallow lakes. *Hydrobiologia*, **317,** 209-220.

Hamm, N.T. and Dade, W.B. (2013) A laboratory study of dynamic sorting of fine, non-cohesive particles by steady, unidirectional currents. *Marine Geology*, **336,** 215-222.

Hartmann, D. (2007) From reality to model: Operationalism and the value chain of particle-size analysis of natural sediments. *Sedimentary Geology*, **202,** 383-401.

Hofmann, H., Lorke, A. and Peeters, F. (2008) The relative importance of wind and ship waves in the littoral zone of a large lake. *Limnology and Oceanography*, **53,** 368.

Holz, C., Stuut, J.-B.W., Henrich, R.d. and Meggers, H. (2007) Variability in terrigenous sedimentation processes off northwest Africa and its relation to climate changes: Inferences from grain-size distributions of a Holocene marine sediment record. *Sedimentary Geology*, **202,** 499-508.

Ijmker, J., Stauch, G., Dietze, E., Hartmann, K., Diekmann, B., Lockot, G., Opitz, S., Wünnemann, B. and Lehmkuhl, F. (2012) Characterisation of transport processes and sedimentary deposits by statistical end-member mixing analysis of terrestrial sediments in the Donggi Cona lake catchment, NE Tibetan Plateau. *Sedimentary Geology*, **281,** 166-179.

Jautzy, J., Ahad, J.M.E., Gobeil, C. and Savard, M.M. (2013) Century-Long Source Apportionment of PAHs in Athabasca Oil Sands Region Lakes Using Diagnostic Ratios and Compound-Specific Carbon Isotope Signatures. *Environmental Science & Technology*, **47,** 6155-6163.

Jin, K. and Ji, Z. (2004) Case Study: Modeling of Sediment Transport and Wind-Wave Impact in Lake Okeechobee. *Journal of Hydraulic Engineering*, **130,** 1055-1067.

Johnson, T.C. and McCave, I.N. (2008) Transport mechanism and paleoclimatic significance of terrigenous silt deposited in varved sediments of an African rift lake. *Limnology and Oceanography*, **53,** 1622-1632.

Kranck, K., Smith, P.C. and Milligan, T.G. (1996a) Grain-size characteristics of fine-grained unflocculated sediments 11: "multi-round" distributions. *Sedimentology*, **43,** 597-606.

Kranck, K., Smith, P.C. and Milligan, T.G. (1996b) Grain-size characteristics of fine-grained unflocculated sediments; I, 'One-round' distributions. *Sedimentology*, **43,** 589-596.

Kværner, J. and Kløve, B. (2008) Generation and regulation of summer runoff in a boreal flat fen. *Journal of Hydrology*, **360,** 15-30.

Laudon, H., Sjöblom, V., Buffam, I., Seibert, J. and Mörth, M. (2007) The role of catchment scale and landscape characteristics for runoff generation of boreal streams. *Journal of Hydrology*, **344,** 198-209.

Law, B.A., Hill, P.S., Milligan, T.G., Curran, K.J., Wiberg, P.L. and Wheatcroft, R.A. (2008) Size sorting of fine-grained sediments during erosion: Results from the western Gulf of Lions. *Continental Shelf Research*, **28,** 1935-1946.

Le Roux, J.P. and Rojas, E.M. (2007) Sediment transport patterns determined from grain size parameters: Overview and state of the art. *Sedimentary Geology*, **202,** 473-488.

Leys, J., McTainsh, G., Koen, T., Mooney, B. and Strong, C. (2005) Testing a statistical curve-fitting procedure for quantifying sediment populations within multi-modal particle-size distributions. *Earth Surface Processes and Landforms*, **30,** 579-590.

Luettich, R.A., Harleman, D.R. and Somlyody, L. (1990) Dynamic behavior of suspended sediment concentrations in a shallow lake perturbed by episodic wind events. *Limnology and Oceanography*, **35,** 1050-1067.

Lwin, T. (2003) Parameterization of Particle Size Distributions by Three Methods. *Mathematical Geology*, **35,** 719-736.

Lyon, S.W., Nathanson, M., Spans, A., Grabs, T., Laudon, H., Temnerud, J., Bishop, K.H. and Seibert, J. (2012) Specific discharge variability in a boreal landscape. *Water Resources Research*, **48,** W08506.

Macumber, A.L., Patterson, R.T., Neville, L.A. and Falck, H. (2011) A sledge microtome for high resolution subsampling of freeze cores. *Journal of Paleolimnology*, **45,** 307-310.

McCave, I.N. and Hall, I.R. (2006) Size sorting in marine muds; processes, pitfalls, and prospects for paleoflow-speed proxies. In: *Geochemistry, Geophysics, Geosystems - G [super 3]*, **7**, pp. @Q10N05-@Q10N05. American Geophysical Union and The Geochemical Society, United States, United States.

McCave, I.N., Manighetti, B. and Beveridge, N.A.S. (1995a) Circulation in the glacial North Atlantic inferred from grain-size measurements. *Nature*, **374,** 149-152.

McCave, I.N., Manighetti, B. and Robinson, S.G. (1995b) Sortable silt and fine sediment size/composition slicing: Parameters for palaeocurrent speed and palaeoceanography. *Paleoceanography*, **10,** 593-610.

McConnachie, J.L. and Petticrew, E.L. (2006) Tracing organic matter sources in riverine suspended sediment: Implications for fine sediment transfers. *Geomorphology*, **79,** 13-26.

McDonald, D.M. and Lamoureux, S.F. (2009) Hydroclimatic and channel snowpack controls over suspended sediment and grain size transport in a High Arctic catchment. *Earth Surface Processes and Landforms*, **34,** 424-436.

McDonald, D.M., Lamoureux, S.F. and Warburton, J. (2010) Assessment of a time-integrated fluvial suspended sediment sampler in a high arctic setting. *Geografiska Annaler. Series A: Physical Geography*, **92,** 225-235.

McLaren, P. and Bowles, D. (1985) The effects of sediment transport on grain-size distributions. *Journal of Sedimentary Research*, **55,** 457-470.

McLaws, I.J. (1980) Silica sands in the Fort McMurray area, Alberta (Ed A.R. Council), **Economic Geology Report 6**, pp. 61. Government of Alberta, Edmonton, Alberta.

McNamara, J.P., Chandler, D., Seyfried, M. and Achet, S. (2005) Soil moisture states, lateral flow, and streamflow generation in a semi-arid, snowmelt-driven catchment. *Hydrological Processes*, **19,** 4023-4038.

Metcalfe, R.A. and Buttle, J.M. (1999) Semi-distributed water balance dynamics in a small boreal forest basin. *Journal of Hydrology*, **226,** 66-87.

Metcalfe, R.A. and Buttle, J.M. (2001) Soil partitioning and surface store controls on spring runoff from a boreal forest peatland basin in north-central Manitoba, Canada. *Hydrological Processes*, **15,** 2305-2324.

Middleton, G.V. (1976) Hydraulic Interpretation of Sand Size Distributions. *The Journal of Geology*, **84,** 405-426.

Middleton, G.V. (1990) Fitting cumulative curves using splines. *Journal of Sedimentary Research*, **60,** 615-616.

Molinaroli, E., Guerzoni, S., De Falco, G., Sarretta, A., Cucco, A., Como, S., Simeone, S., Perilli, A. and Magni, P. (2009) Relationships between hydrodynamic parameters and grain size in two contrasting transitional environments: The Lagoons of Venice and Cabras, Italy. *Sedimentary Geology*, **219,** 196-207.

Murray, M.R. (2002) Is laser particle size determination possible for carbonate-rich lake sediments? *Journal of Paleolimnology*, **27,** 173-183.

PAGES_2k_Consortium (2013) Continental-scale temperature variability during the past two millennia. *Nature Geoscience*, **6,** 339-346.

Påsse, T. (1997) Grain size distribution expressed as tanh-functions. *Sedimentology*, **44,** 1011-1014.

Poizot, E., Méar, Y. and Biscara, L. (2008) Sediment Trend Analysis through the variation of granulometric parameters: A review of theories and applications. *Earth-Science Reviews*, **86,** 15-41.

Pomeroy, J.W., Gray, D.M., Brown, T., Hedstrom, N.R., Quinton, W.L., Granger, R.J. and Carey, S.K. (2007) The cold regions hydrological model: a platform for basing process representation and model structure on physical evidence. *Hydrological Processes*, **21,** 2650-2667.

Qin, X., Cai, B. and Liu, T. (2005) Loess record of the aerodynamic environment in the east Asia monsoon area since 60,000 years before present. *Journal of Geophysical Research: Solid Earth*, **110,** B01204.

Redding, T. and Devito, K. (2011) Aspect and soil textural controls on snowmelt runoff on forested Boreal Plain hillslopes. *Hydrology Research*, **42,** 250-267.

Redding, T.E. and Devito, K.J. (2008) Lateral flow thresholds for aspen forested hillslopes on the Western Boreal Plain, Alberta, Canada. *Hydrological Processes*, **22,** 4287-4300.

Seasolve (2003) *PeakFit: v4 Users Guide*. Seasolve Software Inc., Massachusetts, USA, 255 pp.

Sheridan, M.F., Wohletz, K.H. and Dehn, J. (1987) Discrimination of grain-size subpopulations in pyroclastic deposits. *Geology*, **15,** 367-370.

Shook, K., Pomeroy, J.W., Spence, C. and Boychuk, L. (2013) Storage dynamics simulations in prairie wetland hydrology models: evaluation and parameterization. *Hydrological Processes*, **27,** 1875-1889.

Singer, J.K. and Anderson, J.B. (1984) Use of total grain-size distributions to define bed erosion and transport for poorly sorted sediment undergoing simulated bioturbation. *Marine Geology*, **57,** 335-359.

Slattery, M.C. and Burt, T.P. (1997) Particle size characteristics of suspended sediment in hillslope runoff and stream flow. *Earth Surface Processes and Landforms*, **22,** 705-719.

Sonnenburg, E.P., Boyce, J.I. and Reinhardt, E.G. (2013) Multi-proxy lake sediment record of prehistoric (Paleoindian-Archaic) archaeological paleoenvironments at Rice Lake, Ontario, Canada. *Quaternary Science Reviews*, **73,** 77-92.

Soulsby, R.L., Hamm, L., Klopman, G., Myrhaug, D., Simons, R.R. and Thomas, G.P. (1993) Wave-current interaction within and outside the bottom boundary layer. *Coastal Engineering*, **21,** 41-69.

Sun, D., Bloemendal, J., Rea, D.K., Vandenberghe, J., Jiang, F., An, Z. and Su, R. (2002) Grain-size distribution function of polymodal sediments in hydraulic and aeolian environments, and numerical partitioning of the sedimentary components. *Sedimentary Geology*, **152,** 263-277.

Syvitski, J.P.M. (1991) *Principles, methods, and application of particle size analysis*. Cambridge Univ. Press : New York, NY, United States, United States.

Tanner, W.F. (1964) Modification of sediment size distributions. *Journal of Sedimentary Research*, **34,** 156-164.

Tanner, W.F. (1983) Hydrodynamic origin of Gaussian size distribution. *Proceedings of the Symposium on Coastal Sedimentology*, **6,** 12-34.

van Hengstum, P.J., Reinhardt, E.G., Boyce, J.I. and Clark, C. (2007) Changing sedimentation patterns due to historical land-use change in Frenchman's Bay, Pickering, Canada: evidence from high-resolution textural analysis. *Journal of Paleolimnology*, **37,** 603-618.

Wang, H., Mason, J.A. and Balsam, W.L. (2006) The importance of both geological and pedological processes in control of grain size and sedimentation rates in Peoria Loess. *Geoderma*, **136,** 388-400.

Weltje, G.J. and Prins, M.A. (2003) Muddled or mixed? Inferring palaeoclimate from size distributions of deep-sea clastics. *Sedimentary Geology*, **162,** 39-62.

Weltje, G.J. and Prins, M.A. (2007) Genetically meaningful decomposition of grain-size distributions. *Sedimentary Geology*, **202,** 409-424.

Xiao, J., Chang, Z., Fan, J., Zhou, L., Zhai, D., Wen, R. and Qin, X. (2012) The link between grain-size components and depositional processes in a modern clastic lake. *Sedimentology*, **59,** 1050-1062.

Young, I.R. and Verhagen, L.A. (1996) The growth of fetch limited waves in water of finite depth. Part 1. Total energy and peak frequency. *Coastal Engineering*, **29,** 47-78.

FIGURE CAPTIONS

Figure 1   Map of Canada with the province of Alberta (AB) and the approximate location of Alberta Lake E (ALE; arrowed black square). For details see figure SF1.

Figure 2   Constrained deconvolved and peak fitted grain-size spectra for the ALE freeze core. In each panel the upper portion represents the actual distribution (dotted line) and its approximation (solid line) as the sum of the different log-normal distributions D1 to D6. Also

noted are the modes of each peak, and the goodness of fit statistics [regression least squares coefficient of determination (r^2), standard error (SE), and F-statistic, respectively]. (A) This sample has one of the finest grain-size distributions, with a single fine silt peak at *ca* 11 μm. (B) to (D) medium-grained (B), fine-grained (C) and coarse-grained (D) distributions in three contiguous samples. Similar grain-size spectral variation is present at all levels within the core.

Figure 3   Distributions of the three types of atypical grain-size spectra. The sample depth (in millimetres) refers to the core depth of the figured sample, whilst the bracketed number depicts how many of these spectra occur within the dataset.

Figure 4   Second-order and fourth-order derivative plots of two samples from Figure 2. Solid lines mark the derivative curve with scale on the left-hand y-axis. Dotted lines mark the original spectrum with scale on the right-hand y-axis. The positions of individual distributions are denoted by downward-facing peaks in second-order plots, and upward-facing peaks in fourth-order plots: '2nd' and '4th' denote second-order or fourth-order derivative plots. (A) Second order derivative plot of a fine-grained sample with six distributions. (B) Second-order derivative plot of a relatively coarse-grained sample with D5 denoted by an inflection. (C) Fourth-order derivative plot of the 505 mm sample of (B) where the D5 population denoted in the fourth-derivative. Note that in all derivatives the D1 peak is relatively small in comparison to a tall peak that is a computational artefact generated by the sharp cut-off at the lower limit of the grain-size analysis.

Figure 5   Plot of fit statistics r^2, standard error and F-statistic for determining the most appropriate number of distributions in a model solution. Samples 507 mm and 509 mm were modelled using two to nine log-normal distributions and in this example unconstrained fully-automated deconvolution and peak fitting.. Substantial improvement in the fit statistics (an inflection point) stops at five distributions. However, at five distributions one distribution is wholly contained within another (annotated on the bottom plot are the number of such subservient distributions), indicative of the unrealistic solutions generated by 'unconstrained' fitting (see text). Once D2 to D3 and D4 to D5 separation is forced the plots generate the inflection at six distributions. The '-ve' annotated on the bottom plot represents solutions with negative amplitude distributions. The constrained solutions for these samples are demonstrated in Figure 2B and 2C).

Figure 6   Variation with depth down core of selected variables: (A) D6 Amplitude – note the large spikes at various positions down core, and the ages of different peaks (discussed in text); (B) fine sand; (C) mean grain size; (D) total silt; (E) D3 Area; and (F) medium silt. Grey lines are the individual measurements and the black line represents a nine-point moving average. D3 Area and D6 Amplitude are the complete data as extrapolated by the polynomial algorhythm from the training set.

Figure 7   Cross-plots with regression equations of selected variables from Figure 6: (A) Fine sand versus D6 Amplitude, which is an example of a good, although unlikely, correlation; (B) mean grain size versus D6 Amplitude. For D6 Amplitude <0.7 the data is highly scattered, indicating the region where the mean grain size is probably a composite variable of other grain-

size populations. The reasonable correlation is mostly driven by the higher D6 Amplitude values

that have a considerable impact on mean grain size; (C) D3 Area versus Total Silt. No traditional

grain-size measure can adequately reproduce the D3 Area data. ρ is the Spearmans rank

correlation.

Table 1: Basic statistics for area, amplitude, mode, FWHH, amplitude/FWHH for D1-D6 in the "constrained" model solutions

	units	average	minimum	maximum	SD
D1 Area *	%	8.37	1.65	11.63	1.89
D2 Area *	%	29.57	7.61	44.13	8.16
D3 Area *	%	29.62	12.94	58.68	11.90
D4 Area *	%	18.42	3.77	31.51	8.94
D5 Area *	%	6.45	1.93	17.03	3.57
D6 Area *	%	7.56	2.38	16.83	3.66
D1 Amp	%	0.62	0.12	0.81	0.12
D2 Amp	%	2.07	0.59	2.90	0.47
D3 Amp	%	2.25	0.96	4.67	0.91
D4 Amp	%	1.50	0.32	2.70	0.76
D5 Amp	%	0.53	0.15	1.52	0.33
D6 Amp	%	0.63	0.19	1.45	0.33
D1 Mode (M1)	μm	1.07	0.89	1.37	0.12
D2 Mode (M2)	μm	6.13	5.56	6.48	0.27
D3 Mode (M3)	μm	16.46	12.30	20.80	2.30
D4 Mode (M4)	μm	45.47	35.42	49.54	2.93
D5 Mode (M5)	μm	86.29	80.15	101.40	5.86
D6 Mode (M6)	μm	145.03	130.20	183.57	11.71
D1 FWHH	μm	1.66	1.08	2.47	0.34
D2 FWHH	μm	11.55	6.60	17.27	2.22
D3 FWHH	μm	21.73	15.52	31.92	3.88
D4 FWHH	μm	29.67	16.63	51.67	7.74
D5 FWHH	μm	59.98	22.54	85.88	11.37
D6 FWHH	μm	64.73	48.71	136.44	13.27
Aspect Ratio 1 [t]	%	153%	121%	185%	17%
Aspect Ratio 2 [t]	%	189%	108%	267%	35%
Aspect Ratio 3 [t]	%	132%	102%	191%	17%
Aspect Ratio 4 [t]	%	65%	40%	117%	16%
Aspect Ratio 5 [t]	%	70%	26%	95%	12%
Aspect Ratio 6 [t]	%	44%	33%	74%	6%

SD = standard deviation

* An area calculation for these distributions has units of μm%, and here it is normalised against FWHH to render percentages comparable between the different distributions.

[t] Aspect ratio of these distributions = width per micron grain size ~ FWHH # ÷ Mode # where # = distribution number. Subsequently converted to percentages.

Table 2 Spearman's correlation coefficients for constrained log-normal distributions

2A: Area

	D1 Area	D2 Area	D3 Area	D4 Area	D5 Area	D6 Area
D1 Area	1.00	-0.23	0.23	*-0.44*	-0.25	-0.29
D2 Area	0.11	1.00	***-0.85***	-0.07	-0.16	-0.21
D3 Area	0.10	<0.001	1.00	*-0.32*	-0.05	-0.19
D4 Area	<0.001	0.61	0.02	1.00	***0.53***	***0.84***
D5 Area	0.08	0.26	0.73	<0.001	1.00	***0.70***
D6 Area	0.04	0.14	0.19	<0.001	<0.001	1.00

2B: Amplitude

	D1 Amp	D2 Amp	D3 Amp	D4 Amp	D5 Amp	D6 Amp
D1 Amp	1.00	***0.63***	-0.07	*-0.36*	*-0.40*	*-0.46*
D2 Amp	<0.001	1.00	-0.15	***-0.55***	***-0.53***	***-0.71***
D3 Amp	0.62	0.29	1.00	***-0.60***	*-0.34*	*-0.45*
D4 Amp	0.01	<0.001	<0.001	1.00	***0.61***	***0.84***
D5 Amp	<0.001	<0.001	0.02	<0.001	1.00	***0.73***
D6 Amp	<0.001	<0.001	<0.001	<0.001	<0.001	1.00

2C: Mode

	D1 Mode	D2 Mode	D3 Mode	D4 Mode	D5 Mode	D6 Mode
D1 Mode	1.00	0.04	-0.18	-0.03	0.15	0.31
D2 Mode	0.78	1.00	***0.48***	0.07	0.11	0.02
D3 Mode	0.22	<0.001	1.00	***0.48***	0.18	0.07
D4 Mode	0.85	0.62	<0.001	1.00	0.31	0.19
D5 Mode	0.29	0.45	0.21	0.03	1.00	0.32
D6 Mode	0.03	0.88	0.62	0.19	0.02	1.00

2D: FWHH

	D1	D2	D3	D4	D5	D6
D1	1.00	***-0.74***	-0.16	0.04	0.14	0.42
D2	<0.001	1.00	***0.43***	0.28	-0.08	-0.02
D3	0.27	<0.001	1.00	***0.75***	-0.02	***0.40***
D4	0.81	0.05	<0.001	1.00	-0.13	***0.51***
D5	0.32	0.60	0.89	0.38	1.00	0.30
D6	<0.001	0.90	<0.001	<0.001	0.03	1.00

Spearman's rank correlation coefficients are the numbers in the top-right half of the table, the corresponding statistical significance criteria are in the bottom left of the table; e.g. distribution 3 to 4 area correlation is -0.32 at a significance of $P < 0.02$.
Bold italics signify $P < 0.01$ level, whilst those in italics in 3A and 3B highlight the consistent negative correlation between peaks 1, 2, 3 and peaks 4, 5, 6.

Table 3 Spearmans rank correlation coefficients for calculated grain size population variables D6 Amplitude and D3 Area against conventional summary statistics: mean grain size; total silt, medium silt and fine sand.

3A: Spearmans rank correlation coefficients for individual sample data

	mean GS (μm)	Fine Sand (vol%)	Medium Silt (vol%)	Total Silt (vol%)	D3 Area	D6 Amplitude (vol%)
D3 Area	0.38	*0.00*	0.77	0.54	1.00	*-0.09*
D6 Amplitude (vol%)	0.79	0.96	*-0.02*	-0.80	*-0.09*	1.00

3B: As for A plus using a 9-point moving average to smooth the sample data

	mean GS (μm)	Fine Sand (vol%)	Medium Silt (vol%)	Total Silt (vol%)	D3 Area	D6 Amplitude (vol%)
D3 Area	0.39	*0.03*	0.88	0.63	1.00	*-0.04*
D6 Amplitude (vol%)	0.85	0.98	*-0.04*	-0.71	*-0.04*	1.00

All correlation coefficients are statistically significant at P < 0.01 except for those in itallics
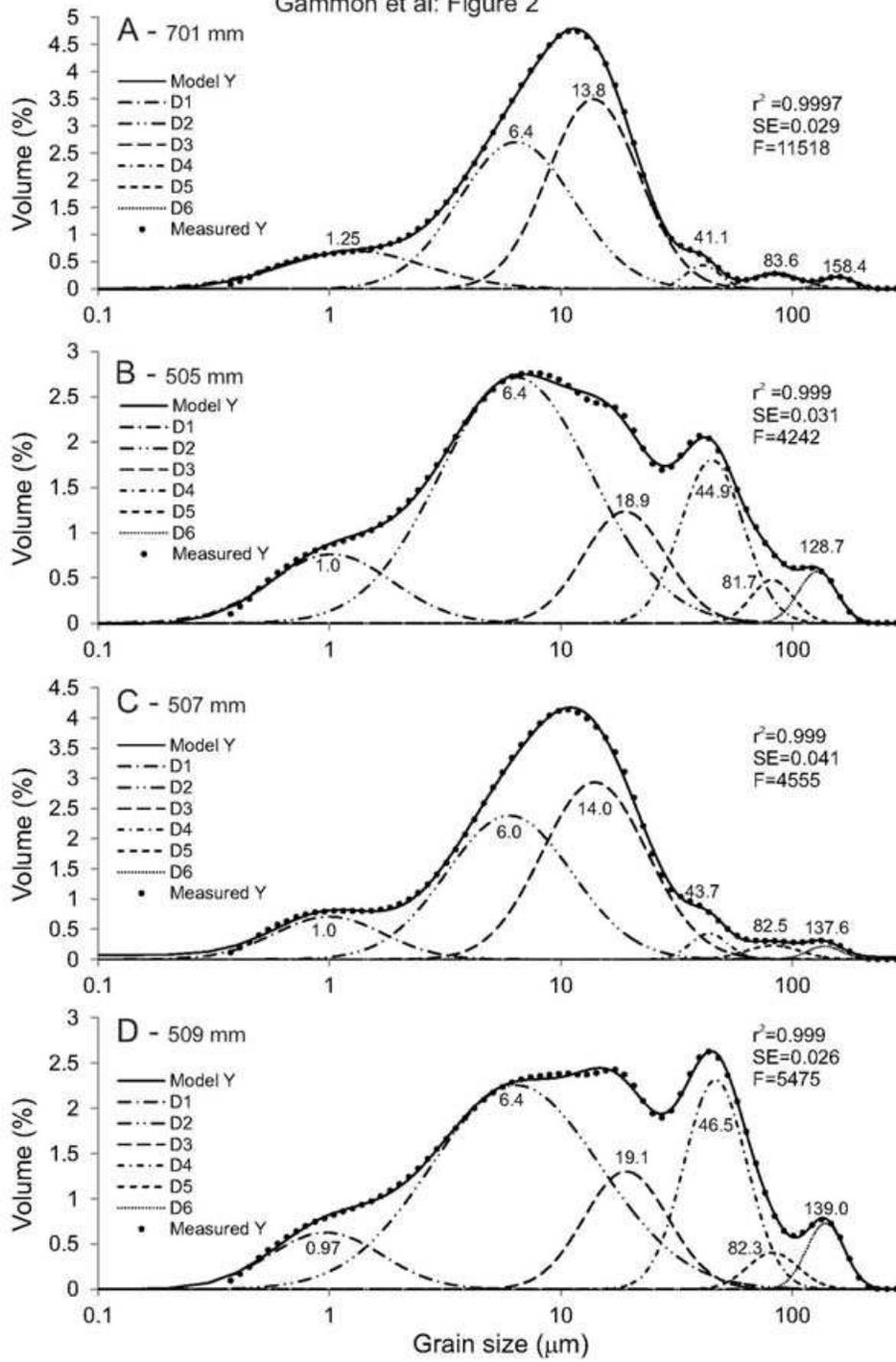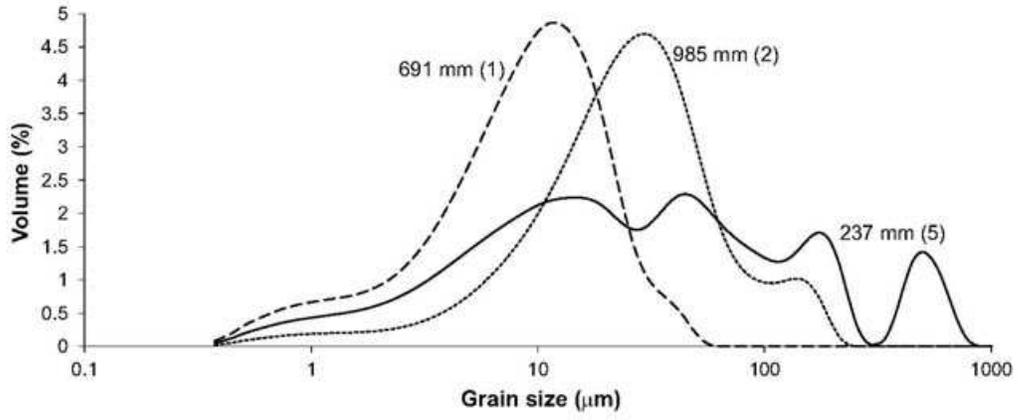GS = grain size; vol% = volume percent
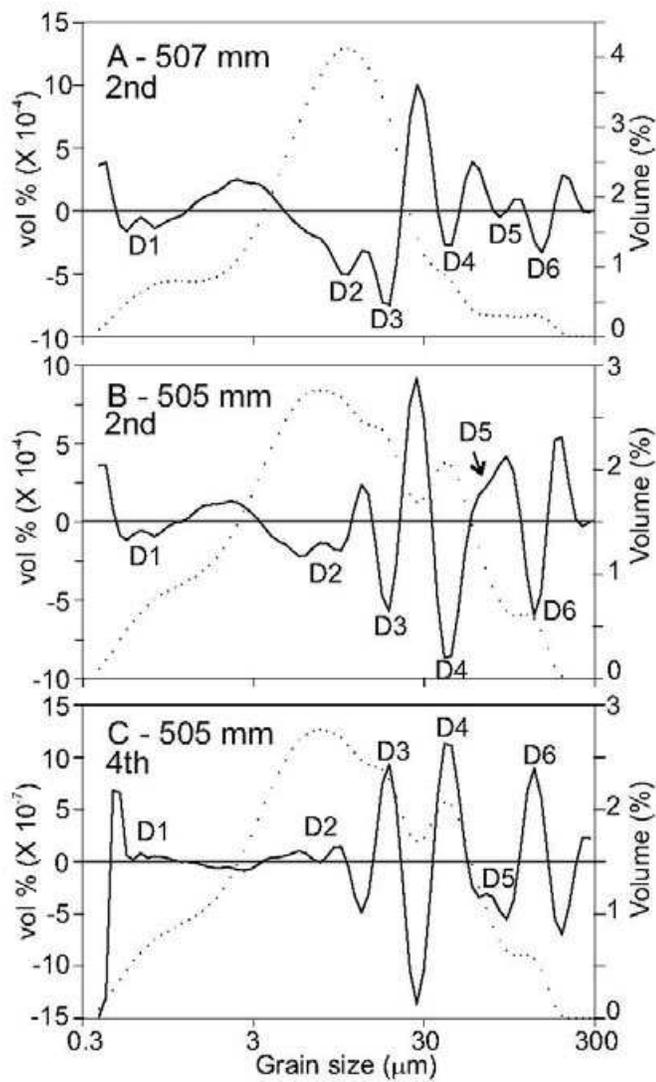

Gammon et al: Figure 1

Location map. Map of Canada with the province of Alberta (AB) and the approximate location of ALE highlighted (arrowed black square).
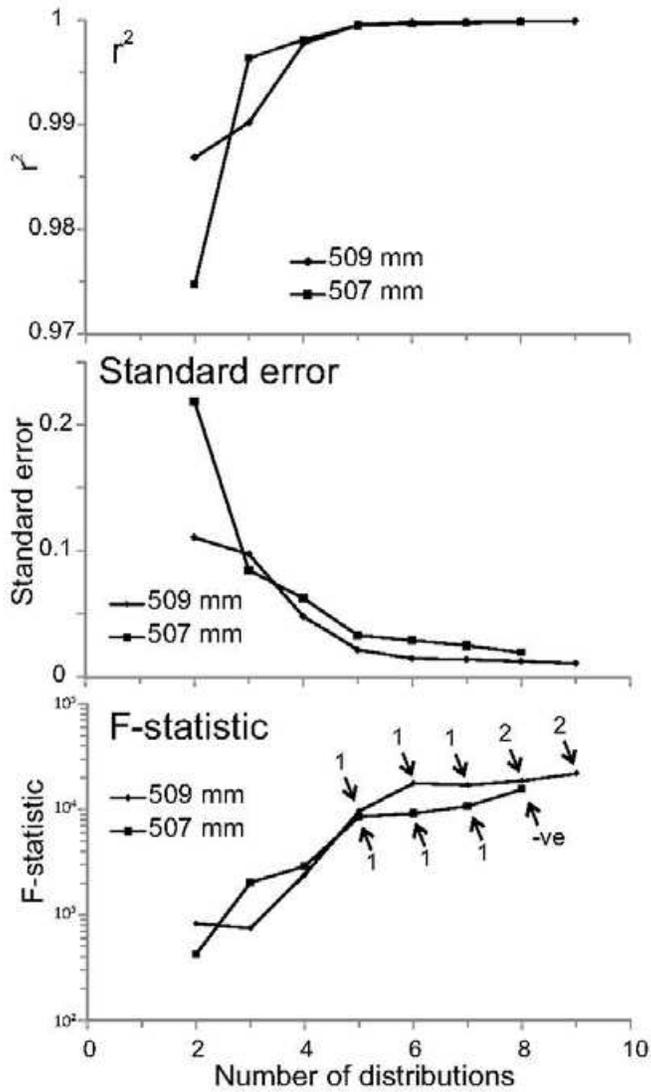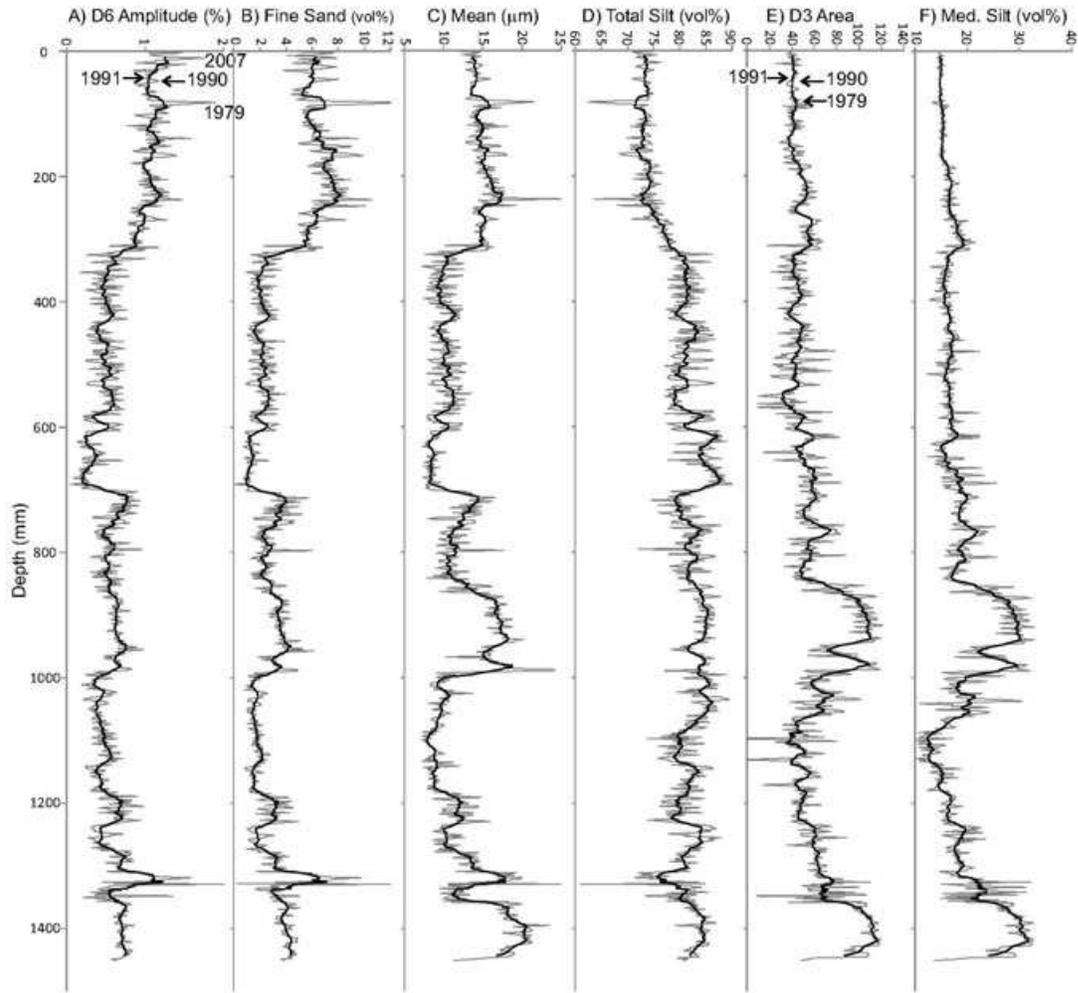
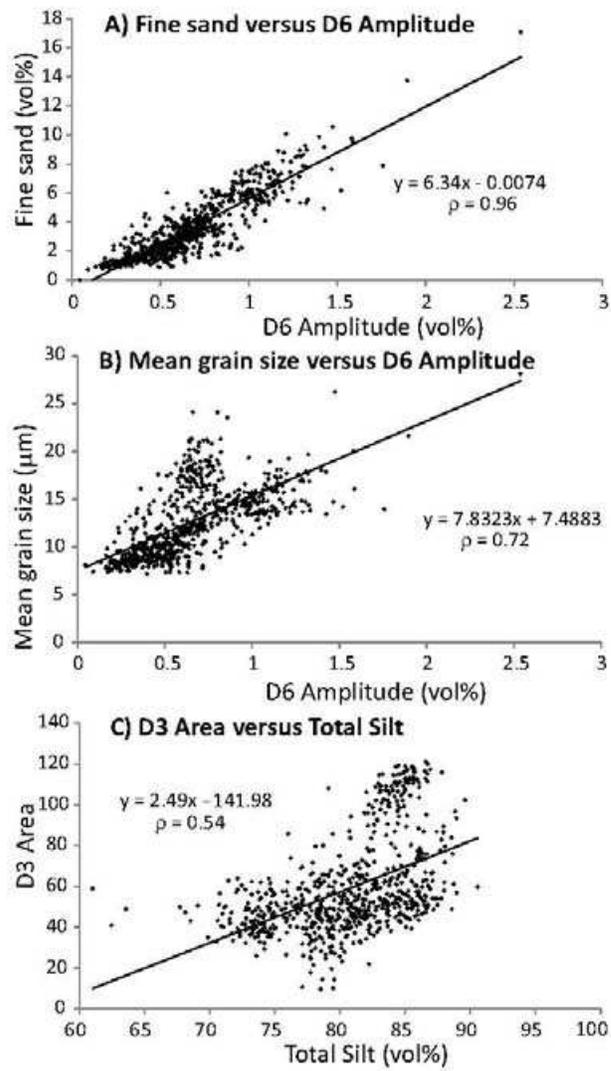Gammon et al: Figure 2

Gammon et al: Figure 3

Gammon et al: Figure 4

Gammon et al: Figure 5

Gammon et al: Figure 6

A) Fine sand versus D6 Amplitude

$y = 6.34x - 0.0074$
$\rho = 0.96$

B) Mean grain size versus D6 Amplitude

$y = 7.8323x + 7.4883$
$\rho = 0.72$

C) D3 Area versus Total Silt

$y = 2.49x - 141.98$
$\rho = 0.54$

Gammon et al: Figure 7